Rapid Communications

Dynamical quantum phase transitions in collapse and revival oscillations of a quenched superfluid

Mateusz Lacki[1] and Markus Heyl[2]

[1]*Instytut Fizyki imienia Mariana Smoluchowskiego, Uniwersytet Jagiellonski, Lojasiewicza 11, 30-048 Krakow, Poland*

[2]*Max-Planck-Institut für Physik komplexer Systeme, 01187 Dresden, Germany*

(Received 7 January 2019; revised manuscript received 28 February 2019; published 18 March 2019)

In this paper, we revisit collapse and revival oscillations in superfluids suddenly quenched by strong local interactions for the case of a one-dimensional Bose-Hubbard model. As the main result, we identify the inherent nonequilibrium quantum many-body character of these oscillations by revealing that they are controlled by a sequence of underlying dynamical quantum phase transitions in the real-time evolution after the quench, which manifest as temporal nonanalyticities in return probabilities or Loschmidt echos. Specifically, we find that the timescale of the collapse and revival oscillations is, first, set by the frequency at which dynamical quantum phase transitions appear, and is, second, of emergent nonequilibrium nature, since it is not only determined by the final Hamiltonian but also depends on the initial condition.

DOI: 10.1103/PhysRevB.99.121107

I. INTRODUCTION

Starting from the observation of collapse and revival oscillations for a Bose-Einstein Condensate matter wave [1], the field of nonequilibrium quantum many-body physics has seen rapid development. Experiments in quantum simulators, such as ultracold atoms or trapped ions, among others [2–5], have in the meantime observed various inherently dynamical quantum phenomena such as prethermalization [6–8], particle-antiparticle production in lattice gauge theories [9], dynamical quantum phase transitions (DQPTs) [10–12], many-body localization [13–15], or discrete time crystals [16–18]. Within the anticipated collapse and revival experiment, a Bose-Einstein condensate (BEC) is suddenly quenched by strong local on-site interactions, which leads to a periodic decay and reappearance of a peaked structure in the bosonic momentum distribution characteristic of a BEC [1] or the visibility of interference patterns [19–21]. While many aspects of this experiment have been theoretically addressed [22–28], it has remained elusive whether there is a general dynamical principle underlying these collapse and revival oscillations, which can explain some central questions that are still unanswered, such as concerning the timescale of these oscillations.

In this paper, we reexamine the collapse and revival oscillations for the case of superfluid order in a one-dimensional Bose-Hubbard model (BHM) subject to a sudden quench of strong local interactions. As for the collapse and revival experiment, we observe a periodic sequence of decay and reappearance of the zero-momentum peak in the bosonic distribution function, see Fig. 1. It is the main result of this paper to identify the collapse and revival oscillations as a genuine nonequilibrium quantum many-body phenomenon (i) by relating them to DQPTs [29–32], and (ii) by revealing the origin and emergent nonequilibrium nature of the associated timescale. Specifically, we find that the collapse and revival oscillations are controlled by a sequence of underlying DQPTs that are characterized by a nonanalytic behavior as a function of time contained in the Loschmidt amplitude,

$$\mathcal{G}(t) = \langle\psi_0|e^{-iHt}|\psi_0\rangle\,, \tag{1}$$

where $|\psi_0\rangle$ denotes the initial condition and H the Hamiltonian driving the quantum real-time dynamics. $\mathcal{G}(t)$ quantifies the amplitude to return to the initial condition and is therefore a natural measure for the collapse and revival of the properties of the initial state such as the zero-momentum peak. As the main result of this paper, we observe that the timescale t_* for the collapse and revival oscillations matches the periodicity at which the system experiences DQPTs. In this way, we provide an explanation of the timescale for these oscillations and link them to a phenomenon that provides general principles of quantum real-time evolution. Importantly, we show that t^* is an emergent nonequilibrium timescale without an equilibrium analog depending both on the initial condition and the final Hamiltonian parameters and therefore t^* is not set, for example, just by the gap of the final Hamiltonian.

II. MODEL AND SETUP

The BHM describes interacting bosons on a lattice close to the aforementioned experiment [1]. We take the underlying lattice to be one-dimensional, yielding the following Hamiltonian:

$$H_{\mathrm{BHM}}(J,U) = -J\sum_{i=1}^{L-1} a_i^\dagger a_{i+1} + a_{i+1}^\dagger a_i + \frac{U}{2}\sum_{i=1}^{L} n_i(n_i-1), \tag{2}$$

where a_i is the annihilation operator for a boson on site i and $n_i = a^\dagger a_i$ the corresponding occupation. The lattice consists of L sites and for convenience we choose open boundary conditions, which, however, has no influence on our main results. The properties of the Hamiltonian $H_{\mathrm{BHM}}(J,U)$ are determined by the dimensionless ratio $s = J/U$ between hopping amplitude J and interaction strength U. At zero temperature, a quantum phase transition of the Kosterlitz-

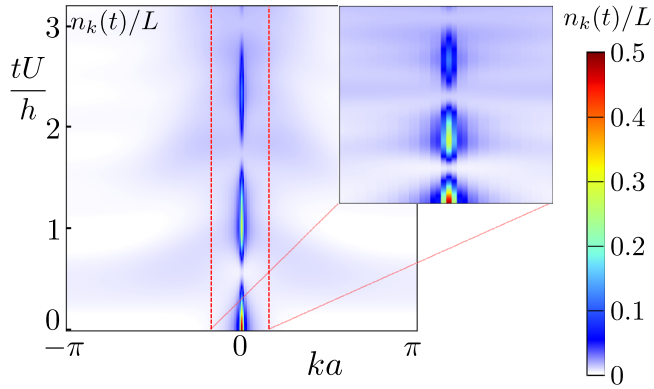

FIG. 1. Collapse and revival oscillations in the real-time evolution of the quasimomentum distribution $n_k(t)$ for a superfluid suddenly quenched by strong local interactions. The system is initially prepared in the superfluid ground state of a one-dimensional Bose-Hubbard model with $L = 120$ lattice sites for modest initial interactions U_i with $s_i = J_i/U_i = 0.36$, where J_i denotes the initial hopping amplitude. After quenching the system suddenly at time $t = 0$ to $s_f = J_f/U = 0.05$, the system exhibits a periodic sequence of collapse and revival oscillations of the zero quasimomentum peak. The inset shows a magnification of the area at low quasimomenta enclosed by the red rectangle.

Thouless type occurs for unit filling at $s_c \approx 0.297$ separating a Mott insulating for $s < s_c$ from a superfluid phase for $s > s_c$ [33–37].

To model the collapse and revival oscillations, we initialize the system in a superfluid ground state $|\psi_0\rangle$ of the BHM for $s > s_c$. At time $t = 0$, the interaction is suddenly quenched to a large value with $s < s_c$ inducing nonequilibrium real-time dynamics which can be formally solved by

$$|\psi_0(t)\rangle = e^{-iHt}|\psi_0\rangle\,, \tag{3}$$

where H denotes the final quenched Hamiltonian.

Just as in the collapse and revival experiment [1] and in related theory papers [26], we study the properties of this quenched system via the quasimomentum distribution,

$$n_k(t) = \langle\psi_0(t)|n_k|\psi_0(t)\rangle\,, \tag{4}$$

where $n_k = b_k^\dagger b_k$ with $b_k = 1/\sqrt{L}\sum_j e^{ijk}a_j$ for $k = -\pi, -\pi + 2\pi/L, \ldots, \pi$. The dynamics of $n_k(t)$ is shown for a representative set of parameters in Fig. 1. Since the system is initially prepared in a superfluid state, the quasimomentum distribution shows a macroscopic occupation at zero momentum $k = 0$. Upon quenching strong local interactions U, $n_k(t)$ exhibits on transient timescales a decay of the superfluid signature at $k = 0$, leading to a spread of occupation across the whole Brillouin zone, see the blue shade in Fig. 1. After this decay, the zero-momentum peak, however, reappears again. This sequence of collapses and revivals continues periodically. In the limit of very strong interactions $s \to 0$, the time-dependence distribution $n_k(t)$ is perfectly periodic in time. For nonzero $0 < s \ll s_c$ instead, the peak height at $n_{k=0}(t)$ exhibits an additional decaying envelope for the subsequent revivals. Still, if the decay time is longer than the revival time, the periodic character of the collapse and revival oscillations is clearly present. This point will be discussed in greater detail later in the main text.

We have obtained this data and the results in the remainder of this paper using numerical simulations based on matrix product state (MPS) techniques. The ground states of the BHM model show sufficiently low entanglement entropy to be accurately represented by MPS [38] with a small bond dimension [39]. The initial ground state we compute by means of thedensity matrix renormalization group algorithm [40]. To perform the real-time evolution of the initial state under the quantum quench we use the time-evolving block decimation (TEBD) [41]. A temporal linear growth of the entanglement entropy limits the maximally achievable evolution time T to $T = 20/U$, up to which our numerics remain accurate. For TEBD, we have used a fourth-order Trotter formula for factorization of the time evolution operator with a time step $\delta t < 0.002/U$. We also note that an MPS representation of vectors allows for accurate computation of very small overlaps, necessary to compute $\mathcal{G}(t)$ without resorting to high-precision linear algebra [38,40]. To ensure convergence of the results, we have determined that further reduction of δt or increasing the bond dimension beyond $m = 200$ used in this paper gives no noticeable improvement on the computed Loschmidt echos.

III. DYNAMICAL QUANTUM PHASE TRANSITIONS

As outlined in the introduction, it is the purpose of this paper to link the collapse and revival oscillations as seen in Fig. 1 to DQPTs and therefore to a genuine nonequilibrium critical phenomenon. Before addressing this connection in detail, let us first outline some basic properties of DQPTs.

The theory of DQPTs provides an extension for the concept of phase transitions to the nonequilibrium dynamical regime [29,31]. While equilibrium transitions are driven by external control parameters such as temperature or pressure, DQPTs are caused solely by the system's internal unitary dynamics. The central object is the Loschmidt amplitude $\mathcal{G}(t)$, see Eq. (1), and the related probability $\mathcal{L}(t) = |\mathcal{G}(t)|^2$ called the Loschmidt echo. Formally, $\mathcal{G}(t)$ resembles equilibrium partition functions at complex parameters [29,31]. Accordingly, it is suitable to introduce dynamical analogs to free-energy densities. In the following, we will consider mainly the dynamical free-energy density $\lambda(t)$ corresponding to the Loschmidt echo $\mathcal{L}(t)$ defined as

$$\lambda(t) = -\frac{1}{L}\log[|\mathcal{G}(t)|^2]\,. \tag{5}$$

As conventional free-energy densities can become nonanalytic at phase transitions, so can the dynamical counterpart $\lambda(t)$ in the thermodynamic limit, but now at critical times, which is the defining feature of DQPTs. Recently, DQPTs and their signatures have been observed experimentally in quantum simulators realized in trapped ions [10], ultracold atoms [12,42], quantum walks [43,44], nanomechanical oscillators [45], and superconducting qubits [46]. It has been shown that many important properties of equilibrium transitions beyond mere nonanalytic behavior are also shared by DQPTs. This includes, for example, their robustness against symmetry-preserving perturbations [47–50]. Moreover, dynamical order

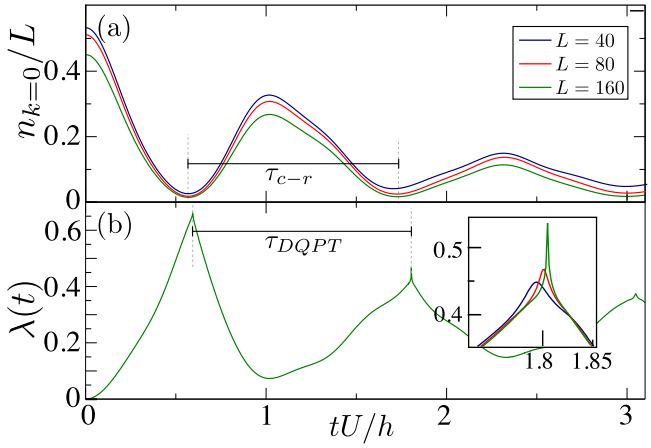

FIG. 2. (a) Real-time evolution of the zero-quasimomentum peak $n_{k=0}(t)$ of the bosonic distribution function for different system sizes and the same parameter values as in Fig. 1, displaying the collapse and revival oscillations. The dashed lines indicate the position of the first two minima of $n_{k=0}(t)$, which defines the timescale τ_{CR}. (b) Dynamics of the Loschmidt echo rate function $\lambda(t)$. The dashed lines mark the location of the first two DQPTs and their temporal distance gives the timescale τ_{DQPT} of the appearance of DQPTs. The inset shows the sharpening for increasing system size L.

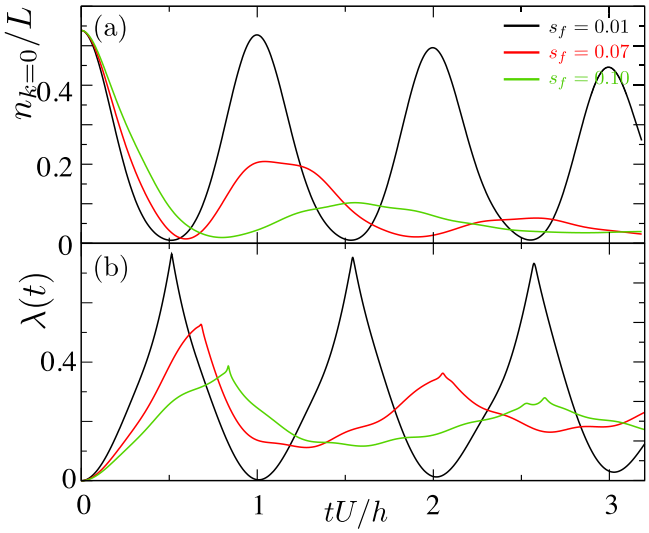

FIG. 3. Dependence of the collapse and revival oscillations as well as the DQPTs as a function of the final Hamiltonian parameter $s_f = J_f/U_f$ at $L = 120$ and $s_i = 0.36$. (a) The dynamics of the zero-quasimomentum peak $n_{k=0}(t)$ exhibits stronger decay and longer oscillation timescales upon increasing s_f. (b) Evolution of the Loschmidt echo rate function $\lambda(t)$ also shows a shift toward larger times of the DQPTs as well as an increased damping for larger s_f.

parameters have been constructed [12,51–56] and measured [12,43,44,46], Landau theories have been formulated [57], as well as scaling and universality have been identified [49,57] for specific models.

IV. RESULTS

Along the lines of our main goal of connecting collapse and revival oscillations to DQPTs, we compare in Fig. 2 the dynamics of the zero-quasimomentum occupation $n_{k=0}(t)$ to the evolution of the dynamical counterpart of the free-energy density $\lambda(t)$ for the same parameters as in Fig. 1. While $n_{k=0}(t)$ shows clearly the discussed collapse and revival oscillations of the superfluid order, $\lambda(t)$ exhibits a sequence of sharp structures in its real-time evolution. Moreover, the location of these sharp features in time appears correlated with the minima in $n_{k=0}(t)$, as we will discuss more quantitatively below.

The sharp structures in time appearing in $\lambda(t)$ become sharper for increasing system size L, as we show for one case in the inset of Fig. 2(b). We conclude that these features eventually turn into nonanalytic kinks in the thermodynamic limit, which is the defining property of a DQPT. Importantly, the system experiences not only a single DQPT in consequence of the considered quantum quench, but rather a whole sequence, the first three of which are contained in the time interval shown in Fig. 2. Clearly, finite-size effects for the kinks become stronger at larger times, so we restrict our analysis to involve only the first two DQPTs. Further, finite-size effects also appear to become more important upon increasing s_i, i.e., when choosing the initial superfluid at weaker interactions, such that we limit ourselves to $s_i \leqslant 1$ in the remainder.

Comparing the time traces of $n_{k=0}(t)$ to $\lambda(t)$ in Fig. 2 already suggests a correlation between the time of collapse, identified with a local minimum of $n_{k=0}(t)$, and the occurrence of a DQPT. We will now study this link more quantitatively by comparing directly the timescales: τ_{CR} for the periodic decay of the zero-quasimomentum peak and τ_{DQPT} for the sequence of DQPTs. We extract τ_{CR} and τ_{DQPT} as indicated in Fig. 2 via the temporal difference between two minima in $n_{k=0}(t)$ and between two DQPTs, respectively.

In Fig. 3(a), we show our numerically obtained data for the zero-quasimomentum occupation $n_{k=0}(t)$ upon varying the parameter s_f of the final Hamiltonian for a fixed initial condition of $s_i = 0.36$. For very small s_f, the collapse and revival oscillations are very prominent. Upon increasing s_f, the oscillation period grows together with faster decay of the signal. Starting from $s_f = 0.1$, this reduces the visibility of the collapse and revival pattern making it difficult to resolve τ_{CR}. We limit our discussion in the following only to those cases where the oscillations are significantly visible for the first two collapses. In Fig. 3(b), we additionally show our obtained data for the dynamical free-energy density $\lambda(t)$. In this case, the ratio of maximal to minimal value of the $\lambda(t)$ decreases as well with larger s_f. This alone does not impair our ability to extract τ_{DQPT} even for relatively large $s_f \approx 0.1$, unlike τ_{CR}.

What becomes a challenge is that typically for larger s_f the function $\lambda(t)$ has a tendency to become smoother, requiring larger values of L to locate a nonanalytic peak. The time at which it occurs is also defined by the fact that except narrow time intervals around DQPTs, the function $\lambda(t)$ is practically L-independent. The size of these intervals shrinks as L is increased [see inset of Fig. 2(b)]. This provides an estimate of location of the DQPT.

In Fig. 4, we now compare the timescales τ_{CR} and τ_{DQPT} as defined in Fig. 2. We plot these as a function of the final parameters s_f for three initial conditions given by $s_i =$

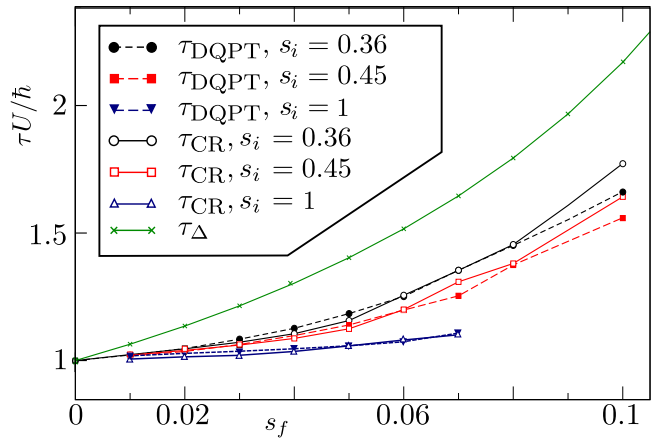

FIG. 4. Comparison of the timescale for the collapse and revival oscillations τ_{CR} and the timescale $\tau_{\rm DQPT}$ for DQPTs for different initial conditions s_i as a function of the final Hamiltonian parameter s_f at $L = 120$. The dashed and solid lines show τ_{CR} and $\tau_{\rm DQPT}$, respectively. The different colors blue, red, and black refer to different initial conditions $s_i = 0.36, 0.45, 1.0$. The fine-dashed curve displays the equilibrium timescale $\tau_\Delta = 2\pi/\Delta$ set by the gap Δ of the final Hamiltonian.

0.36, 0.45, 1. In addition, we include as a reference also the timescale $\tau_\Delta = 2\pi\hbar/\Delta$ associated with the gap Δ of the final Hamiltonian. For $s_f = 0$, the collapse and revival oscillations occur with a period $\tau_{CR} = 2\pi\hbar/U$ [1,26], which is just a consequence of the discrete equidistant spectrum of the Hamiltonian $H_f = U\sum_l n_l(n_l - 1)$. Consequently, all the timescales have to agree in this limit, as one can also clearly identify in Fig. 4. Upon increasing s_f, one can see corrections to the $s_f = 0$ limit. Here, τ_{CR} and $\tau_{\rm DQPT}$ stay close to each other while τ_Δ deviates significantly. However, we observe slight deviations between τ_{CR} and $\tau_{\rm DQPT}$ which we attribute to three possible origins: (i) finite-size effects that lead to slight shifts of both of the timescales, as one can already see from Fig. 2, (ii) the reduced visibility of the collapse and revival signal upon increasing s_f as discussed before, and (iii) slight systematic shifts in estimating oscillation frequencies from the first two minima for damped signals. Clearly, however, τ_{CR} and $\tau_{\rm DQPT}$ go hand in hand with each other whereas τ_Δ behaves completely differently. Further, τ_{CR} and $\tau_{\rm DQPT}$ exhibit a marked influence of the initial conditions. All these observations suggest that the collapse and revival oscillations are associated with an *emergent nonequilibrium timescale* with no equilibrium counterpart. Since this nontrivial timescale also appears in the nonanalyticities of the Loschmidt echo, we conclude that these oscillations are controlled by a sequence of underlying DQPTs. This interpretation aligns well with previous papers that have found a relation between order parameter dynamics and DQPTs in other models [29,51,58–61] as well as in a recent experiment [10].

V. CONCLUDING DISCUSSION

Closed nonequilibrium quantum many-body systems cannot be characterized by thermodynamic means. On the one hand, this allows us to relax equilibrium constraints such as the equal *a priori* probability of the microcanonical ensemble, which can lead to quantum states with properties that are inaccessible in a thermodynamic context such as time crystals, for instance [16,17,62–65]. On the other hand, this shifts the theoretical description from the Hamiltonian level to a more challenging one at the time evolution operators $U(t)$ level. This can be seen, for instance, from one central result of our paper, which is that the collapse and revival oscillations are described by an emergent nonequilibrium timescale that is not only determined by the properties of the final Hamiltonian but also depends on the initial condition. Most importantly, studying $U(t)$ adds an additional scale into the problem, which is time t itself. The theory of DQPTs provides a general framework to incorporate time explicitly and to study the properties of time evolution operators $U(t)$, since, for instance, the central object $\mathcal{G}(t)$ can be interpreted as a matrix element of $U(t)$.

Recently, quenches and DQPTs in related models exhibiting collapse and revival oscillations for states breaking a continuous symmetry have been investigated in other contexts [28,59]. For the work on the $O(N)$ model [59], an extension of the Loschmidt echo to the case of a broken continuous symmetry has been proposed in terms of the full return probability to the ground-state manifold, involving projections of the time-evolved state to all states within the ground-state manifold. This appears different at first sight from the scenario we study in the present paper, since we only consider a single overlap. Importantly, however, we have chosen a setup with a fixed particle number according to the experimental situation [1,26] where the conjugate phase is undefined. Therefore, the initial condition constitutes a superposition including all states in the degenerate ground-state manifold and thereby all the projections are naturally included. While the close connection between the order parameter dynamics and DQPTs has also been observed for many other models exhibiting a discrete symmetry breaking [10,29,51,58–61,66–68], a recent paper has questioned this connection for specific models exhibiting a superfluid to Mott insulator transition in equilibrium [28]. Although we also study a system with such a transition, it is important to emphasize a central difference making a direct comparison challenging, which is the underlying integrability of the models studied in Ref. [28]. These therefore exhibit stable modes, as their elementary excitations don't show scattering as opposed to our case, which leads to a much more complex dynamics. And this appears to be a crucial aspect since we find evidence that, beyond the atomic limit, the collapse and revival oscillations in our model are an inherent quantum many-body phenomenon that cannot be related to an approximation involving independent stable modes.

The initial experiment has been performed in a three-dimensional optical lattice [1]. Our theoretical considerations use a chain instead, leading immediately to the question of how our results might extend to higher dimensions and, in particular, whether the oscillations are similarly related to DQPTs. This cannot be addressed by means of the MPS formalism used here. Recently, however, DQPTs in Ising models beyond the one-dimensional limit have been studied using exact diagonalization techniques [69] and a stochastic approach to nonequilibrium quantum real-time dynamics [69]. In the future, the simulation of two-dimensional systems might, in principle, be within reach of projected-entangled pair states

[70]. However, let us emphasize that the Loschmidt echo still naturally provides a measure for the departure from and return to the initial superfluid state and therefore of the collapse and revival oscillations.

While collapse and revival oscillations can be experimentally accessed straightforwardly using time-of-flight imaging [2], measuring Loschmidt amplitudes or echos remains a challenge. Recently, however, the return probability, i.e., Loschmidt echo, for condensed bosons in an ultracold atom setup has been estimated [8], which gives hope that our theoretical predictions might become observable in the near future.

ACKNOWLEDGMENTS

We thank W. Zwerger for important initializing discussions that led to this paper, J. Lang for valuable comments on the paper, as well as D. Delande and J. Zakrzewski for the TEBD code. This work was realized under National Science Center (Poland) Project No. 2016/23/D/ST2/00721 and was supported in part by PL-Grid Infrastructure. Financial support by the Deutsche Forschungsgemeinschaft (DFG) via the Gottfried Wilhelm Leibniz Prize program is gratefully acknowledged.

[1] M. Greiner, O. Mandel, T. W. Hänsch, and I. Bloch, Nature **419**, 51 (2002).
[2] I. Bloch, J. Dalibard, and W. Zwerger, Rev. Mod. Phys. **80**, 885 (2008).
[3] I. Bloch, J. Dalibard, and S. Nascimbène, Nat. Phys. **8**, 267 (2012).
[4] R. Blatt and C. F. Roos, Nat. Phys. **8**, 277 (2012).
[5] I. M. Georgescu, S. Ashhab, and F. Nori, Rev. Mod. Phys. **86**, 153 (2014).
[6] M. Gring, M. Kuhnert, T. Langen, T. Kitagawa, B. Rauer, M. Schreitl, I. Mazets, D. A. Smith, E. Demler, and J. Schmiedmayer, Science **337**, 1318 (2012).
[7] B. Neyenhuis, J. Zhang, P. W. Hess, J. Smith, A. C. Lee, P. Richerme, Z.-X. Gong, A. V. Gorshkov, and C. Monroe, Sci. Adv. **3** (2017).
[8] K. Singh, K. M. Fujiwara, Z. A. Geiger, E. Q. Simmons, M. Lipatov, A. Cao, P. Dotti, S. V. Rajagopal, R. Senaratne, T. Shimasaki, M. Heyl, A. Eckardt, and D. M. Weld, arXiv:1809.05554.
[9] E. A. Martinez, C. A. Muschik, P. Schindler, D. Nigg, A. Erhard, M. Heyl, P. Hauke, M. Dalmonte, T. Monz, P. Zoller, and R. Blatt, Nature **534**, 516 (2016).
[10] P. Jurcevic, H. Shen, P. Hauke, C. Maier, T. Brydges, C. Hempel, B. P. Lanyon, M. Heyl, R. Blatt, and C. F. Roos, Phys. Rev. Lett. **119**, 080501 (2017).
[11] J. Zhang, G. Pagano, P. W. Hess, A. Kyprianidis, P. Becker, H. Kaplan, A. V. Gorshkov, Z.-X. Gong, and C. Monroe, Nature **551**, 601 (2017).
[12] N. Fläschner, D. Vogel, M. Tarnowski, B. Rem, D.-S. Lühmann, M. Heyl, J. Budich, L. Mathey, K. Sengstock, and C. Weitenberg, Nat. Phys. **14**, 265 (2018).
[13] M. Schreiber, S. S. Hodgman, P. Bordia, H. P. Lüschen, M. H. Fischer, R. Vosk, E. Altman, U. Schneider, and I. Bloch, Science **349**, 842 (2015).
[14] J. Smith, A. Lee, P. Richerme, B. Neyenhuis, P. W. Hess, P. Hauke, M. Heyl, D. A. Huse, and C. Monroe, Nat. Phys. **12**, 907 (2016).
[15] J.-y. Choi, S. Hild, J. Zeiher, P. Schauß, A. Rubio-Abadal, T. Yefsah, V. Khemani, D. A. Huse, I. Bloch, and C. Gross, Science **352**, 1547 (2016).
[16] J. Zhang, P. W. Hess, A. Kyprianidis, P. Becker, A. Lee, J. Smith, G. Pagano, I. D. Potirniche, A. C. Potter, A. Vishwanath, N. Y. Yao, and C. Monroe, Nature **543**, 217 (2017).
[17] S. Choi, J. Choi, R. Landig, G. Kucsko, H. Zhou, J. Isoya, F. Jelezko, S. Onoda, H. Sumiya, V. Khemani, C. von Keyserlingk, N. Y. Yao, E. Demler, and M. D. Lukin, Nature **543**, 221 (2017).
[18] A. Kosior and K. Sacha, Phys. Rev. A **97**, 053621 (2018).
[19] M. Anderlini, J. Sebby-Strabley, J. Kruse, J. V. Porto, and W. D. Phillips, J. Phys. B **39**, S199 (2006).
[20] J. Sebby-Strabley, B. L. Brown, M. Anderlini, P. J. Lee, W. D. Phillips, J. V. Porto, and P. R. Johnson, Phys. Rev. Lett. **98**, 200405 (2007).
[21] S. Will, T. Best, U. Schneider, L. Hackermüller, D.-S. Lühmann, and I. Bloch, Nature **465**, 197 (2010).
[22] C. Kollath, A. M. Läuchli, and E. Altman, Phys. Rev. Lett. **98**, 180601 (2007).
[23] U. R. Fischer and R. Schützhold, Phys. Rev. A **78**, 061603 (2008).
[24] P. Johnson, E. Tiesinga, J. V. Porto, and C. J. Williams, New J. Phys. **11**, 093022 (2009).
[25] F. A. Wolf, I. Hen, and M. Rigol, Phys. Rev. A **82**, 043601 (2010).
[26] J. Schachenmayer, A. J. Daley, and P. Zoller, Phys. Rev. A **83**, 043614 (2011).
[27] U. R. Fischer and B. Xiong, Phys. Rev. A **84**, 063635 (2011).
[28] T. Fogarty, A. Usui, T. Busch, A. Silva, and J. Goold, New J. Phys. **19**, 113018 (2017).
[29] M. Heyl, A. Polkovnikov, and S. Kehrein, Phys. Rev. Lett. **110**, 135704 (2013).
[30] A. A. Zvyagin, Low Temp. Phys. **42**, 971 (2016).
[31] M. Heyl, Rep. Prog. Phys. **81**, 054001 (2018).
[32] M. Heyl, arXiv:1811.02575.
[33] T. D. Kühner and H. Monien, Phys. Rev. B **58**, R14741(R) (1998).
[34] J. Zakrzewski and D. Delande, in *Let's Face Chaos Through Nonlinear Dynamics: Proceedings of "Let's Face Chaos Through Nonlinear Dynamics" 7th International Summer School and Conference*, edited by M. Robnik and V. Romanovski, AIP Conf. Proc. No. 1076 (AIP, New York, 2008), p. 292.
[35] S. Rachel, N. Laflorencie, H. F. Song, and K. Le Hur, Phys. Rev. Lett. **108**, 116401 (2012).
[36] J. Carrasquilla, S. R. Manmana, and M. Rigol, Phys. Rev. A **87**, 043606 (2013).
[37] K. V. Krutitsky, Phys. Rep. **607**, 1 (2016).
[38] U. Schollwöck, Ann. Phys. **326**, 96 (2011).
[39] We consider bond dimension of $m = 160$ and $n_{\max} = 7$ bosons per site.
[40] G. De Chiara, M. Rizzi, D. Rossini, and S. Montangero, J. Comput. Theor. Nanosci. **5**, 1277 (2008).
[41] G. Vidal, Phys. Rev. Lett. **91**, 147902 (2003).

[42] C. Hainaut, P. Fang, A. Rancon, J.-F. Clément, P. Szriftgiser, J.-C. Garreau, C. Tian, and R. Chicireanu, Phys. Rev. Lett. **121**, 134101 (2018).
[43] K. Wang, X. Qiu, L. Xiao, X. Zhan, Z. Bian, W. Yi, and P. Xue, Phys. Rev. Lett. **122**, 020501 (2019).
[44] X.-Y. Xu, Q.-Q. Wang, M. Heyl, J. C. Budich, W.-W. Pan, Z. Chen, M. Jan, K. Sun, J.-S. Xu, Y.-J. Han, C.-F. Li, and G.-C. Guo, arXiv:1808.03930.
[45] T. Tian, Y. Ke, L. Zhang, S. Lin, Z. Shi, P. Huang, C. Lee, and J. Du, arXiv:1807.04483.
[46] X.-Y. Guo, C. Yang, Y. Zeng, Y. Peng, H.-K. Li, H. Deng, Y.-R. Jin, S. Chen, D. Zheng, and H. Fan, arXiv:1806.09269.
[47] C. Karrasch and D. Schuricht, Phys. Rev. B **87**, 195104 (2013).
[48] J. N. Kriel, C. Karrasch, and S. Kehrein, Phys. Rev. B **90**, 125106 (2014).
[49] M. Heyl, Phys. Rev. Lett. **115**, 140602 (2015).
[50] S. Sharma, S. Suzuki, and A. Dutta, Phys. Rev. B **92**, 104306 (2015).
[51] J. C. Budich and M. Heyl, Phys. Rev. B **93**, 085416 (2016).
[52] S. Sharma, U. Divakaran, A. Polkovnikov, and A. Dutta, Phys. Rev. B **93**, 144306 (2016).
[53] U. Bhattacharya and A. Dutta, Phys. Rev. B **96**, 014302 (2017).
[54] U. Bhattacharya, S. Bandyopadhyay, and A. Dutta, Phys. Rev. B **96**, 180303 (2017).
[55] U. Bhattacharya and A. Dutta, Phys. Rev. B **95**, 184307 (2017).
[56] M. Heyl and J. C. Budich, Phys. Rev. B **96**, 180304 (2017).
[57] D. Trapin and M. Heyl, Phys. Rev. B **97**, 174303 (2018).
[58] M. Heyl, Phys. Rev. Lett. **113**, 205701 (2014).
[59] S. A. Weidinger, M. Heyl, A. Silva, and M. Knap, Phys. Rev. B **96**, 134313 (2017).
[60] B. Žunkovič, M. Heyl, M. Knap, and A. Silva, Phys. Rev. Lett. **120**, 130601 (2018).
[61] Y.-P. Huang, D. Banerjee, and M. Heyl, arXiv:1808.07874.
[62] V. Khemani, A. Lazarides, R. Moessner, and S. L. Sondhi, Phys. Rev. Lett. **116**, 250401 (2016).
[63] D. V. Else, B. Bauer, and C. Nayak, Phys. Rev. Lett. **117**, 090402 (2016).
[64] K. Sacha, Phys. Rev. A **91**, 033617 (2015).
[65] K. Sacha and J. Zakrzewski, Rep. Prog. Phys. **81**, 016401 (2017).
[66] I. Homrighausen, N. O. Abeling, V. Zauner-Stauber, and J. C. Halimeh, Phys. Rev. B **96**, 104436 (2017).
[67] J. Lang, B. Frank, and J. C. Halimeh, Phys. Rev. B **97**, 174401 (2018).
[68] J. C. Halimeh, M. Van Damme, V. Zauner-Stauber, and L. Vanderstraeten, arXiv:1810.07187.
[69] S. De Nicola, B. Doyon, and M. J. Bhaseen, J. Phys. A: Math. Theor. **52**, 05LT02 (2019).
[70] F. Verstraete, V. Murg, and J. I. Cirac, Adv. Phys. **57**, 143 (2008).